

RAPID COMMUNICATION

Constructing optimized wire electrodes for fiber supercapacitors



Bin Liu^{a,b}, Boyang Liu^b, Xianfu Wang^b, Di Chen^b,
Zhiyong Fan^{c,*}, Guozhen Shen^{a,*}

^aState Key Laboratory for Superlattices and Microstructures, Institute of Semiconductors, Chinese Academy of Sciences, Beijing 100083, PR China

^bWuhan National Laboratory for Optoelectronics (WNLO) and College of Optical and Electronic Information, Huazhong University of Science and Technology, Wuhan 430074, PR China

^cDepartment of Electronic and Computer Engineering, Hong Kong University of Science and Technology, Clear Water Bay, Kowloon, Hong Kong, PR China

Received 5 June 2014; received in revised form 10 August 2014; accepted 28 August 2014
Available online 8 September 2014

KEYWORDS

Fiber supercapacitor;
Optimized;
Wire electrode;
Mn₂O₃ cubes;
Flexible

Abstract

Fiber electronic devices are commonly built on fibrous substrates with the advantages for the direct use as weavable and embedded device units or integrated textile modules. In this work, Mn₂O₃ cube-arrays/carbon wire electrodes were designed for a new kind of fiber supercapacitors. To realize micro-devices with well-optimized performance, different electrode structures were designed and fabricated including the straight, bent, and coiled fiber supercapacitors (S-FSC, B-FSC, and C-FSC), among which the C-FSC showed the optimized and best performance. Our work confirmed that the performance of micro-devices can be well tuned by simply tailoring the device architectures.

© 2014 Elsevier Ltd. All rights reserved.

Introduction

As integration, miniaturization, flexibility, and optimization are considered as the primary features of the new generation

of electronics, enormous effort has been paid on developing flexible and wearable devices in recent years [1–12]. Different from conventional two-dimensional planar electronics, fiber electronic devices are commonly built on one-dimensional fibrous/wire substrates. Fiber electronic devices usually show advantages for the direct use as wearable and embedded device units or integrated textile modules that cannot be fulfilled by conventional planar devices, which are very attractive in realizing miniaturized portable devices and

*Corresponding authors.

E-mail addresses: dichen@mail.hust.edu.cn (D. Chen), eezfan@ust.hk (Z. Fan), gzshen@semi.ac.cn (G. Shen).

multi-functional “smart textiles” for sensors, detectors, displays and implanted medical devices. Several kinds of fiber electronic devices have been designed including fiber logic circuits [13], fiber solar cells [14,15], fiber displays [16], and fiber nanogenerators [17], etc.

The development of fiber electronic devices inspired much interest in developing efficient, lightweight, highly flexible/wearable energy storage devices such as fiber solar cells, fiber lithium ion batteries, and fiber supercapacitors (FSC) since they are one of the key components for fully flexible electronic systems. Among the emerged fiber energy devices, fiber supercapacitors have higher power density, longer cycling life and more safe operation than fiber lithium ion batteries and thus are considered as a new class of energy storage components. Since Wang's group reported the first prototype of FSC made from ZnO nanowires [18], FSCs made of different electrodes were designed. For examples, Peng et al. designed FSC by twisting two aligned MWCNT fibers [19]. Miao et al. fabricated yarn FSCs based on CNT@PANI arrays [20]. To better prevent the twisted fiber-electrodes from electric short during bending, Zou et al. demonstrated the well-designed helical spacer wire placed in between two electrodes [21]. Our group also fabricated FSCs made of ZnCo_2O_4 nanowires electrode and grapheme electrode [22].

Although different kinds of FSCs with different performances were successfully designed recently, one key and crucial issue that was neglected is how to improve the performance of each FSC. As is known, Mn_2O_3 has many unique advantages in energy storage fields, such as low cost, environmentally friendly, and high potential performance, etc. Although many methods have been developed to synthesize various Mn_2O_3 electrodes for supercapacitors under different experimental conditions, such as particles, nanorods, and spheres [23-25], no information about Mn_2O_3 cube/carbon fiber-electrodes prepared via a low-cost/facile route was disclosed till now. Herein, with Mn_2O_3 cube arrays/carbon fibers as electrodes, we demonstrated that the performance of the designed FSCs can be efficiently improved by simply varying the electrode structure (straight, bent, and coiled fiber electrodes, respectively). Both experiments and theoretical simulations were carried out to demonstrate the efficient strategy to get optimized FSCs.

Experimental section

Synthesis of Mn_2O_3 cube-arrays/carbon fibers matrix

$\text{Mn}(\text{AC})_2$ (2 mmol) and urea (2 mmol) was initially dissolved in distilled water (40 mL) and then the solution was transferred into a Teflon-lined autoclave. Pre-cleaned carbon fibers were then immersed in this solution. A typical hydrothermal reaction at 160 °C for 5 h was then performed, which resulted in the formation of the aligned Mn_2O_3 cube arrays grown on the carbon fibers. The morphology and microstructure of the samples were investigated by field emission scanning electron microscopy (FE-SEM; Sirion 200).

Wire-device fabrication and characterization

After placing two as-synthesized composite fibers as working electrodes on a PET film, the silver electrodes were

fixed to the two ends of the PET substrate. A gel electrolyte of PVA/ H_2SO_4 was transferred on the composite fibers to form a thin all-solid-state device. CV characteristics of the fiber supercapacitors were evaluated by sweeping the voltage from 0 to 0.8 V at various scan rates using a CHI electrochemical station (760D). Galvanostatic charge-discharge curves of these devices were measured at different current densities between 0 and 0.8 V using a PVA/ H_2SO_4 gel electrolyte with the electrochemical station at the room temperature.

Computational simulations

The simulations of the capacitors were carried out by using ANSYS Maxwell. To calculate the capacity, the width of each electrode was set as 1 mm, and the length of the capacitors, the distance between two electrodes were set as 50 mm and 2 mm, respectively. In addition, the voltages on the two fiber electrodes are symmetrically set as +0.4 V and -0.4 V.

Results and discussion

We first grew Mn_2O_3 cube arrays on carbon fibers to form the binder-free fiber electrodes via a simple hydrothermal method, as is shown in Figure 1a. Briefly, carbon fibers with excellent electrical conductivity were used as the templates for the in-situ growth of Mn_2O_3 cube-arrays (Figure S1). The experimental details can be found in Experimental section. Figure 1b shows the low-magnification scanning electron microscopy (SEM) image of the as-prepared Mn_2O_3 cube-arrays/carbon fibers from the hydrothermal method for 5 h, which clearly shows that the samples consist of several small fibers coated with Mn_2O_3 crystals. Higher-magnification SEM image shown in Figure 1c reveals that numerous microcubes grown on the carbon fibers are packed tightly, forming high density shells on the carbon fibers. Figure 1d displays that the as-prepared Mn_2O_3 microcubes have highly uniform size of about 2 μm and the diameter of individual core/shell composite fiber is approximately 14 μm , which is slightly larger than that of the bare carbon fibers due to the coating of Mn_2O_3 product. Figure 1e shows the photograph of a single as-grown composite fiber coiled around a glass rod, revealing its outstanding flexibility.

To acquire information about the composition of the as-grown product, energy dispersive spectroscopy (EDS) micro-analysis was carried out on the selected area of an individual composite fiber, as shown in Figure S2a. The corresponding EDS spectrum revealed that the as-grown structures are composed of only C, Mn, and O elements, indicating formation of pure Mn_2O_3 /carbon fibers matrix (Figure S2b). The information about the elemental distributions within the composite fiber is provided by EDS mapping and the corresponding images of C, Mn and O are shown in Figure S2(c-e) respectively. Note that all the images show that the corresponding element is distributed uniformly across the whole wire, further confirming the uniform Mn_2O_3 /C core/shell structures are successfully prepared. In addition, the crystallographic structure of the as-prepared composites was further analyzed by X-ray diffraction (XRD) (Figure S3). All the diffraction peaks in this

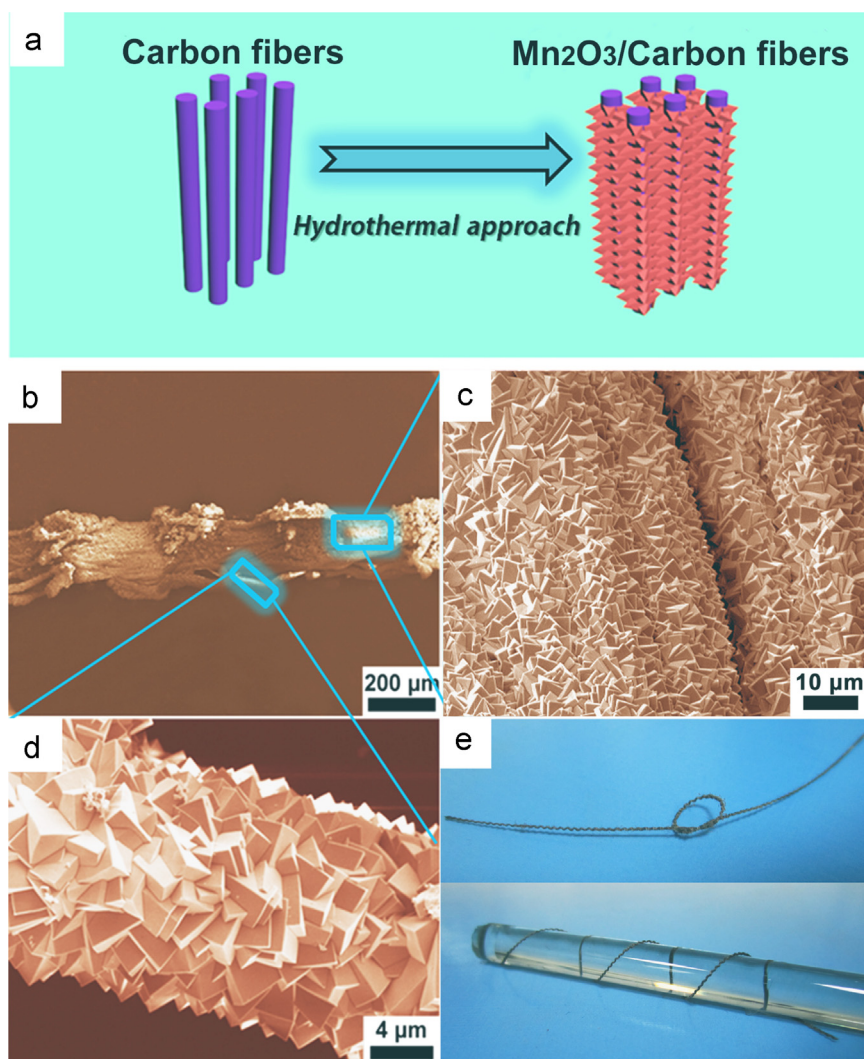


Figure 1 Sample fabrication and morphology characterization. (a) Schematic of the material synthesis via a facile hydrothermal approach. (b-d) SEM images of the Mn₂O₃ cube-arrays/carbon fibers composites. (e) Photographs of the looped (upper photo) and the coiled (lower photo, around the glass rod) as-grown composite fibers.

pattern can be readily indexed as cubic-phase Mn₂O₃, which are consistent with the values in the standard card (JCPDS Card no. 41-1442) [26]. Meanwhile, the peaks at around 26° and 43° can be attributed to the carbon templates.

With the demonstration of uniform structures and excellent flexibility, the as-synthesized Mn₂O₃ cube-arrays/carbon fiber structures may find applications as the core building blocks for flexible energy storage devices. Herein, an intriguing new class energy storage unit, i.e. all-solid-state flexible fiber supercapacitors, was fabricated by integrating two of as-grown composite fibers as the electrodes on flexible PET substrate. To optimize the electrochemical performance of the micro-devices, three types of wire-supercapacitors were fabricated, namely, the straight fiber supercapacitor (S-FSC), the bent fiber supercapacitor (B-FSC), and the coiled fiber supercapacitors (C-FSC). Figure 2(a-c) shows the photographs of the S-FSC, B-FSC, and C-FSC on PET substrates, respectively. With flexible fiber-shaped electrodes and ultrathin thickness, the as-prepared devices showed excellent flexibility as evidenced in Figure 2d-f, where the C-FSC was fixed on an optical table

and mechanically bent to various angles. Apparently, the flexible, thin, and light-weight features enable integration of the as-fabricated devices on clothing or other objects (Figure S4), thus can greatly facilitate various emerging wearable/portable applications. Schematics in Figure 2g depict the device structures of the flexible fiber supercapacitors. Briefly, two of the as-prepared Mn₂O₃ cube-arrays/carbon composite fibers as active materials were first fixed on PET substrate with Ag slurry as the conducting electrodes. Then, the composite fibers were coated with the PVA/H₂SO₄ gel-electrolyte to complete fiber supercapacitor fabrication. To investigate their unique electrochemical properties, the CV measurements of these devices were carried out at various scanning rates of 10, 20, 30, 40, and 50 mV s⁻¹ with a voltage range from 0 to 0.8 V. As shown in Figure 3h-j, the CV curves of all three devices, i.e. S-FSC, B-FSC, and C-FSC, with L: 50 mm, D: 2 mm (L: wire length; D: inter-wire distance) present the typical capacitive characteristics. From the plots, it can be observed that the symmetrical rectangular-shape CV curves of C-FSC indicate a close to ideal capacitive behavior (Figure 2j) [27-30].

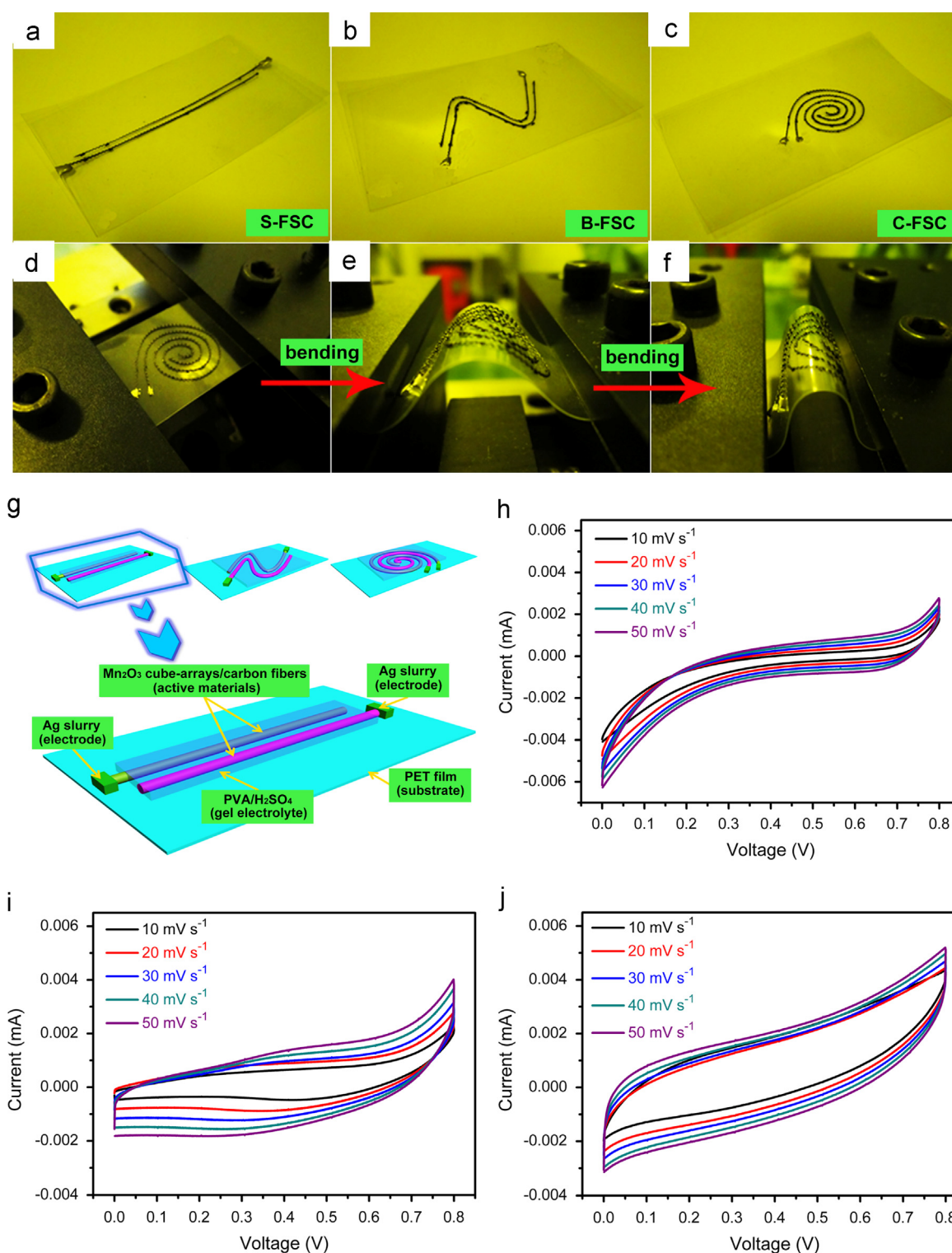


Figure 2 Fiber-device demonstration and electrochemical characteristics of the as-fabricated fiber-supercapacitors measured at various scan rates between 0 and 0.8 V. Photographs of (a, b and c) three as-fabricated fiber-devices: S-FSC, B-FSC, and C-FSC respectively, and (d-f) bending process of a C-FSC device. (g) Schematics of different architectures of three devices, showing several components of these micro-supercapacitors. Cyclic voltammetry of these devices based on Mn₂O₃ cube-arrays/carbon fibers electrodes measured between 0 and 0.8 V at various scan rates. Three mini-type fiber-supercapacitors: (h) S-FSC, (i) B-FSC, and (j) C-FSC.

It reveals the composite electrodes in this work are mainly described as a double-layer behavior that includes physical charge-adsorption on the surface of active-materials not

chemical reactions on electrodes during charge-discharge process. This common phenomenon is observed in many symmetric supercapacitors reported previously [22,30-32].

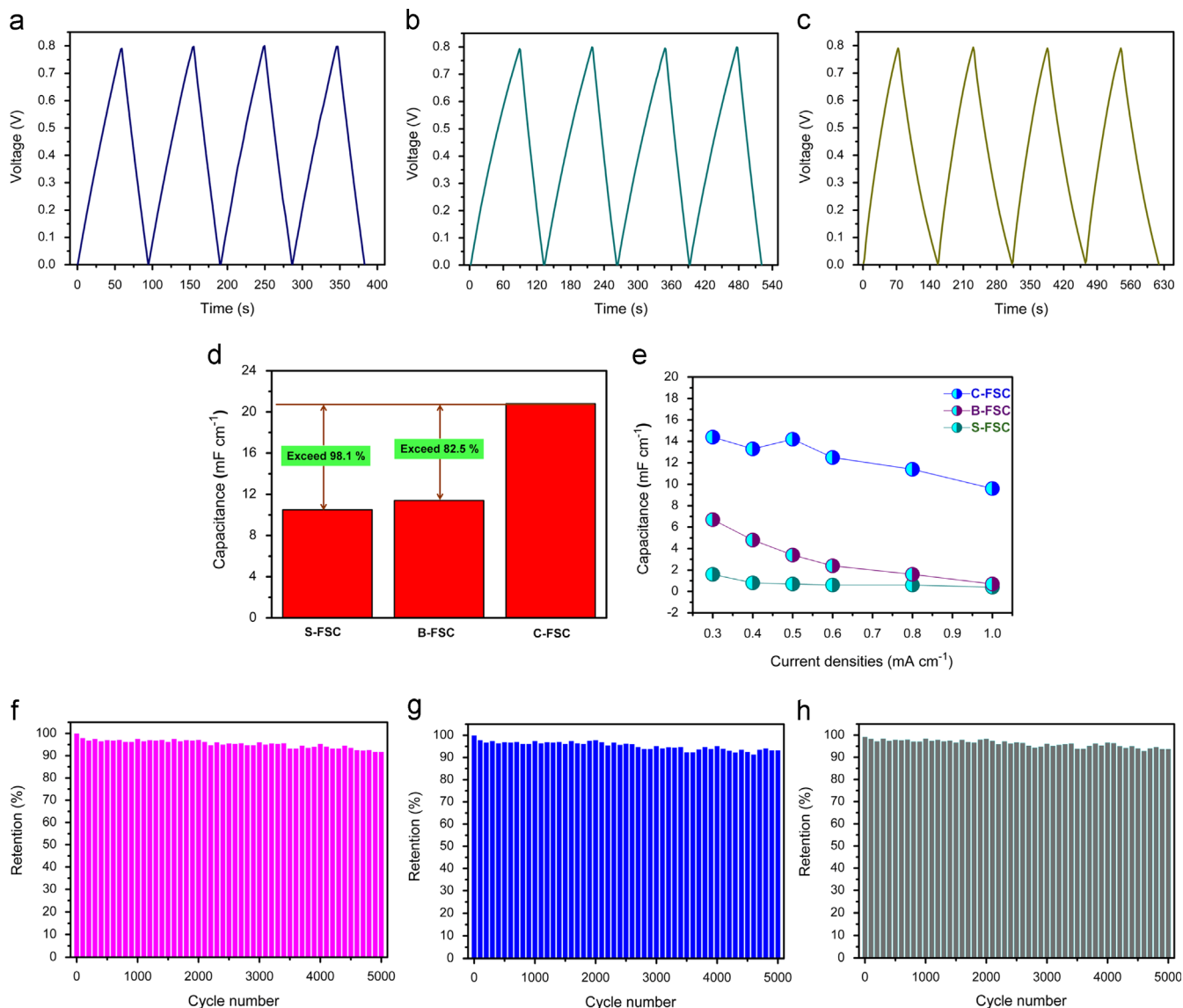


Figure 3 Electrochemical characterizations of S-FSC, B-FSC, and C-FSC. (a-c) Typical charge/discharge curves cycled at 0.2 mA cm^{-1} between 0 and 0.8 V for the first 4 cycles, (d) a histogram of the capacitance for the three devices, and (e) the rate-capability comparison. Cycling performance for (f) S-FSC, (g) B-FSC, and (h) C-FSC with up to 5000 charge/discharge cycles at 0.2 mA cm^{-1} .

Furthermore, the curve area of C-FSC is much larger than that of B-FSC and S-FSC, thus demonstrates its superior electrochemical properties.

To further investigate the performance of the three devices, we have characterized their charge-discharge behaviors under galvanostatic conditions with a voltage range from 0 to 0.8 V. As shown in Figure 3a-c, the first 4 cycles of all three devices represent high cycling stability and efficient charge storage. The discharging time of C-FSC is significantly increased when compared with that of both B-FSC and S-FSC, revealing that the C-FSC device has a much higher capacity, which is consistent with the above CV results. The discharge profiles of the S-FSC devices and device with pure carbon fiber electrodes only were also investigated, as shown in Figure S5. Since the contribution of the carbon fibers electrodes to the capacitance is negligible, we can draw the conclusion that the total

capacitance can be primarily attributed to the loaded Mn_2O_3 materials in our micro-supercapacitor.

The capacitances of the devices can be calculated according to the following equation:

$$C_L (\text{mF cm}^{-1}) = I \Delta t / L \Delta V$$

where I refers to the current density used for the charge/discharge measurements, Δt refers to the time elapsed for the discharge cycle, L denotes the effective length of the wire electrodes, and ΔV represents the voltage interval of the discharge measurement. Calculated from this equation, the capacitances of S-FSC, B-FSC, and C-FSC are 2.1 mF cm^{-1} , 2.3 mF cm^{-1} , and 4.2 mF cm^{-1} , respectively. The capacitance of the C-FSC is about 100% and 83% higher than that of the S-FSC and B-FSC, as also revealed in Figure 3d. The rate-performance of the three devices was also investigated. The capacitances of these devices are calculated

from each discharge curves at various current densities of 0.3, 0.4, 0.5, 0.6, 0.8, and 1.0 mA cm⁻¹, respectively. The corresponding results are summarized in Figure 3e. Clearly, the C-FSC shows the best rate performance among all three devices.

Since the cycling performance is a crucial parameter for a typical capacitor, it is important to study the retention of capacitances cycled over numerous times. Figure 3f, g and h demonstrate the cycling performance of the S-FSC, B-FSC, and C-FSC for as many as 5000 charge/discharge cycles at 0.2 mA cm⁻¹, the results show that the retention of S-FSC, B-FSC, and C-FSC can maintain as high as 91%, 93%, and 94% after 5000 charge/discharge cycles, respectively, indicating the excellent cycling stability of all the three devices. Therefore, all the above results indicate that our fabricated unique fiber supercapacitors possess superior performance, which is crucial for high-performance electronics.

The effects of electrode distance and length on the performance were also studied and the corresponding results are demonstrated in Figures S6 and S7, and Table S1. From these data we can observe that, when the lengths of the electrodes for all three assembled S-FSC, B-FSC, and C-FSC devices were the same and the distance of the electrodes increased from 1.5 mm to 2 mm and 2.5 mm, the corresponding capacitance decreased gradually (Figure 4a). Also, the corresponding capacitances of each

device increased with the increase of the electrode lengths from 50 mm to 150 mm when keeping the distance between the electrodes the same (Figure 4b).

To further reveal the origin of the better performance for C-FSC as compared to S-FSC and B-FSC, theoretical modeling was carried out by using ANSYS Maxwell software. Figure 5(a-c) illustrates the models of fiber supercapacitors in three novel configurations: straight fibers, bent fibers, and coiled fibers, respectively, with the actual models shown in Figures S8-10. Figure 5(d-f) demonstrates the electrostatic potential distribution around the S-FSC, B-FSC, and C-FSC devices with +0.4 V and -0.4 V voltage applied to the two electrodes. From these results we can see that the potential distributions of the straight and bending parts for fiber electrodes are obviously different among the three fiber supercapacitors. The potential distribution of the entire area of C-FSC is similar to that of bending points of B-FSC. Their corresponding energy distributions are provided in Figure 5g-i. It can be also seen that the energy densities increase with the change of color ranging from blue to red in the simulation results. Figure 5(j-l) shows the three equivalent areas from S-FSC, B-FSC, and C-FSC, revealing that C-FSC has more high-energy areas and homogeneous energy-distributions compared with S-FSC and B-FSC. Furthermore, the energy densities (E) are associated with capacitance (C) for each supercapacitor according to the following equations:

$$dE = dQ \cdot V$$

$$C = \frac{Q}{V}$$

$$dE = V^2 dC$$

$$C = \sum dC$$

where E (J), Q (C), V (V), and C (F) refer to the energy density, quantity of electric charge, voltage, and capacitance, respectively. As a result, the relative capacitances of C-FSC and B-FSC are 1.51 and 1.08 times of S-FSC, respectively, indicating that C-FSC enables more fiber electrodes to participate in the charge-discharge processes. It can be revealed that C-FSC has far higher capacitance than the other two modules (B-FSC and S-FSC), which is well consistent with the above experiment results. This is attributed to the various assembled electrode-arrangements that can result in variation of their corresponding capacitances.

We further analyzed C-FSC devices with different fiber length (L) and inter-fiber distance (D) combinations, including L 50 mm, D 1.5 mm, L 50 mm, D 2.5 mm, L 100 mm, D 2 mm, and L 150 mm, D 2 mm with modeling (Figure S11). For the change of electrode distance of C-FSC, the relative capacitance ratio of three models (D 1.5 mm, D 2 mm, and D 2.5 mm) is 1.4:1:0.8, respectively (Figure 6a). The capacitance of CWS devices shows an obvious rising trend as the inter-electrode distance decreases. Also, based on the original fiber-device (L 50 mm, D 2 mm), the related simulations were expanded to longer fiber length devices (L 100 mm, D 2 mm, and L 150 mm, D 2 mm). The relative capacitance ratio of above three models including L 50 mm, L 100 mm, and L 150 mm is 1:2.2:3.4, respectively (Figure 6b), showing that longer electrode can lead to more capacitance with the same inter-electrode distance in the case of C-FSC. However, beyond the effect of electrode distance and length on the capacitance, the unique coiled design is the key for

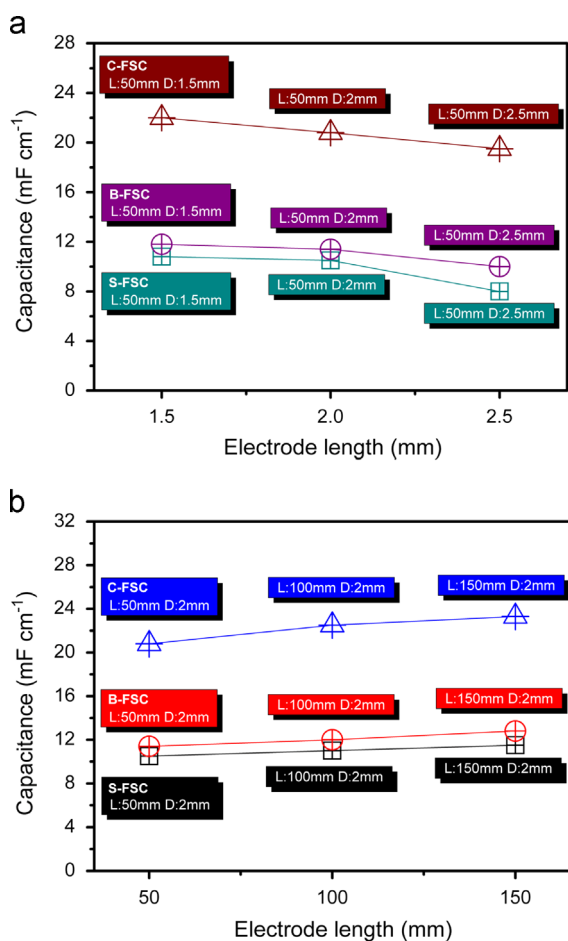


Figure 4 Capacitances for the assembled fiber-devices with different (a) electrode distance and (b) electrode length.

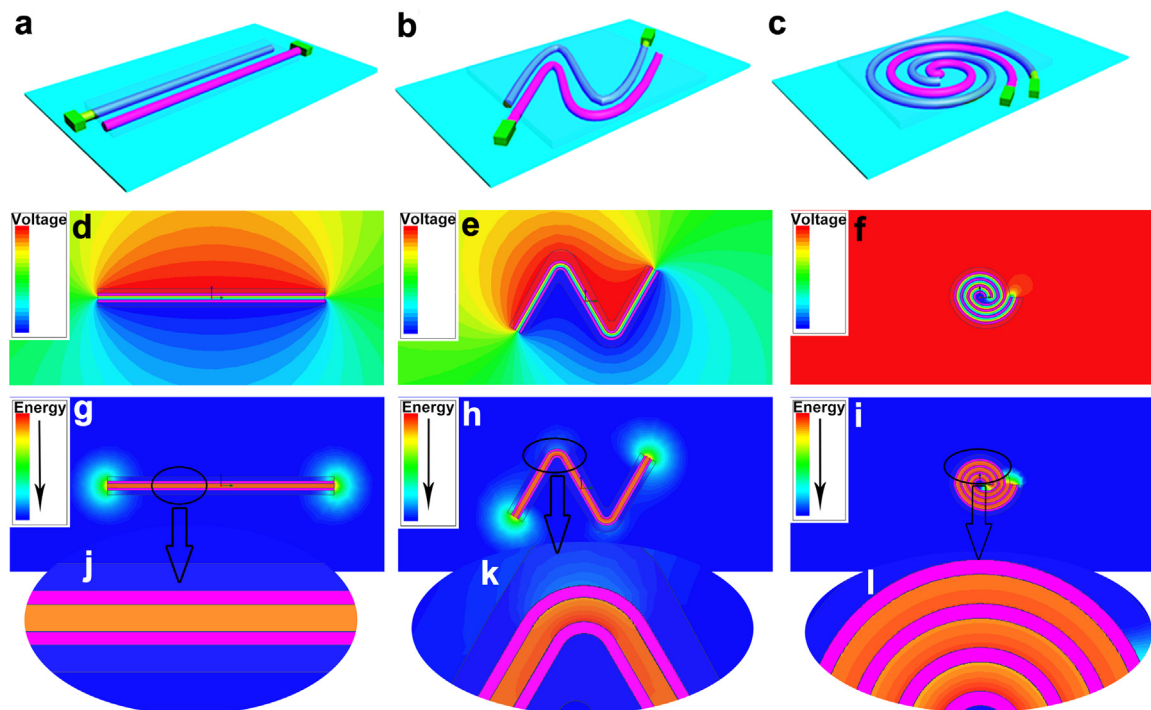


Figure 5 Various fiber supercapacitors based on Mn_2O_3 cube-arrays/carbon fibers matrix, such as S-FSC (a), B-FSC (b), and C-FSC (c). The simulations of voltage (d-f), and energy distributions (g-l) of S-FSC, B-FSC, and C-FSC, respectively.

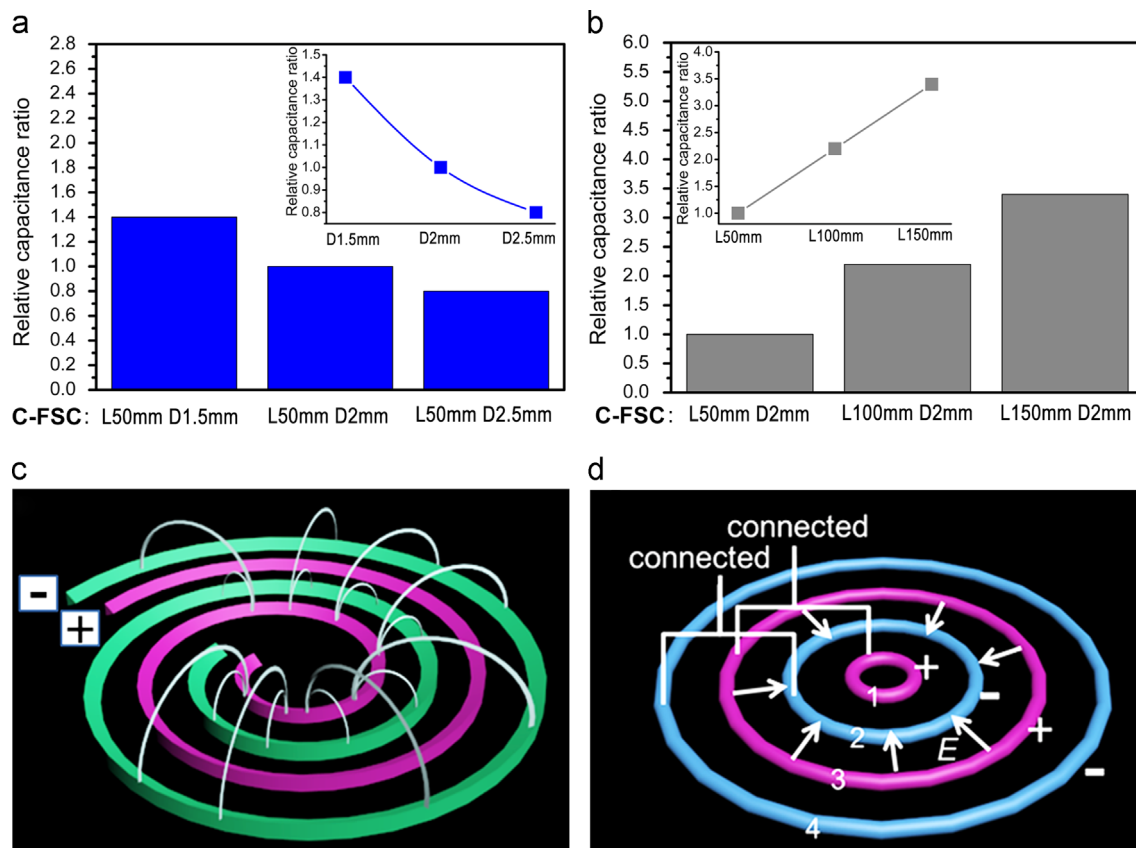


Figure 6 Simulated results of various electrode distance and length and analysis of unique merits of circled fiber supercapacitors (C-FSC). (a, b) Simulated relative capacitance ratio among C-FSC devices with different electrode distance (D1.5 mm, D2.0 mm, and D2.5 mm), and with electrode length (L50 mm, L100 mm, and L150 mm), respectively. (c) The distributed capacitance effect. (d) The approximate model in electric field.

the high capacitance and energy storage capacity. From the above results, we have discovered that, by designing devices with different configurations, we can easily tune the capacitance and rate performances of the devices though all the three devices use similar electrodes with the same amount of active materials. Since the three types of micro-supercapacitors have electrodes with the same length and distance, one may draw the conclusion that they should have the same capacitance. However, increased capacitance was observed for the C-FSC devices in our experiments. We attribute this fact to the synergetic effects of the coiled fiber electrode configuration for the C-FSC device, which can be explained as follows. For the C-FSC, its compact design can lead to close to ideal space-utilization and the maximized total capacitance, due to the coupling among the non-adjacent fiber electrodes with the opposite polarity, as shown in Figure 6c. Compared with S-FSC, B-FSC, and C-FSC involves more portions of fiber electrodes to participate in charge-discharge processes, which results in well-optimized performance of C-FSC in terms of capacitance and rate stability. To further explain higher capacity of C-FSC as compared to S-FSC and B-FSC, a simplified model of C-FSC was built, as shown in Figure 6d. For a single round ring capacitor with one pair of inner and outer fiber electrodes, typically only the electric field between the two electrodes need to be considered. And, the weak electric field outside the rings can be ignored. In Figure 6d, if the electric field between the ring electrode 2 and 3 is ignored temporarily, the C-FSC can be regarded as a parallel connected two single round ring capacitors. S-FSC can also be treated as two separated straight line capacitors, as shown in Figure S12. Here, both S-FSC and C-FSC have same average length and these simplified approximate models were demonstrated to better make some qualitative analysis of fiber-devices. From the plot, it can be seen that the total capacitance of a C-FSC is the same with that of a S-FSC. According to the Gauss Law:

$$\oint_S \rightarrow E \cdot d \rightarrow S = \frac{1}{\epsilon} q$$

where E refers to the electric field intensity on an arbitrary closed surface S , ϵ refers to the permittivity, and q refers to the total electric charge surrounded by the closed surface. For the devices with two electrodes with the same length and distance, the capacitances of a straight line and a ring capacitor should be same. However, once the electric field between ring electrodes 2 and 3 is considered, the integral of the electric field intensity through the Gaussian surface will be increased, and the negative electric charge on ring electrode 2 will be increased as well, so is the positive charge on ring electrode 3. While the electric field distribution in between ring electrodes 1 and 2, 3 and 4 does not change, leading to the unaltered electric charge on ring electrodes 1 and 4. These naturally results in higher capacitance and more charge stored of a C-FSC device, as compared to a S-FSC and a B-FSC, due to their simple and non-optimized structures. Hence, all these results indicate that novel C-FSC presented here can achieve desired well-optimized properties.

In addition, the fundamental formula that determines the capacitance of a capacitor is illustrated as follows: $C = (\epsilon S) / 4\pi kd$, where C is the capacitance of the capacitor, ϵ is the dielectric constant of the material between the electrodes,

S is the surface area of one electrode, k is electrostatic constant, and d is the distance between two electrodes. Considering the definite thickness of the three-dimensional electrodes, the wire-shaped supercapacitors can also be approximatively analyzed as parallel combinations of plate-capacitors. Here, for the effect of electrostatic equilibrium, the electron charges are only distributed on the inside surface of the electrodes of S-FSC and B-FSC. But for the C-FSC, the electron charges are distributed on the both inside and outside surface of its electrodes (except for the innermost/outmost ring). As a result, for the same length and distance of electrodes, the effective surface area (S) of C-FSC is much larger than the other two devices, thus revealing that optimized C-FSC can achieve the highest capacitance among these devices.

Conclusions

In summary, here we report a novel flexible Mn_2O_3 cube-arrays/carbon fiber structure that has been fabricated into straight, bent, and coiled fiber supercapacitors on flexible PET substrates. These flexible devices based on micro-fibers demonstrated desirable capacitive behaviors, excellent cycling life-time, and high rate-capacity. Among all three types of devices, the C-FSC delivered the highest capacitance and best rate-capability as compared with the S-FSC and B-FSC, due to its unique compact configuration. Our results also revealed that the inter-electrode distance and length can affect the performance of the devices. Overall, the fiber supercapacitors demonstrated here may satisfy the increasing demands on reliable power sources for next-generation electronics which requires flexibility and portability.

Acknowledgments

This work was supported by the National Natural Science Foundation of China (91123008, 61377033) and the 973 Program of China (2011CB933300).

Appendix A. Supporting information

Supplementary data associated with this article can be found in the online version at <http://dx.doi.org/10.1016/j.nanoen.2014.08.021>.

References

- [1] D. Khang, H. Jiang, Y. Huang, J.A. Rogers, *Science* 311 (2006) 208.
- [2] Z. Jiang, W. Xie, M. Li, B. Podobnik, W. Zhou, H. Stanley, *Proc. Natl. Acad. Sci. USA* 110 (2013) 1600.
- [3] Y. Cui, C.M. Lieber, *Science* 291 (2001) 851.
- [4] Y. Cui, Z. Zhong, D. Wang, W. Wang, C.M. Lieber, *Nano Lett.* 3 (2003) 149.
- [5] S. Xu, Y. Zhang, J. Cho, J. Lee, X. Huang, L. Jia, J. Fan, Y. Su, J. Su, H. Zhang, H. Cheng, B. Lu, C. Yu, C. Chuang, T. Kim, T. Song, K. Shigeta, S. Kang, C. Dagdeviren, I. Petrov, P. V. Braun, Y. Huang, U. Paik, J.A. Rogers, *Nat. Commun.* 4 (2013) 1543.
- [6] B. Liu, J. Zhang, X. Wang, G. Chen, D. Chen, C. Zhou, G. Shen, *Nano Lett.* 12 (2012) 3005.

- [7] B. Liu, X. Wang, H. Chen, Z. Wang, D. Chen, Y. Cheng, C. Zhou, G. Shen, *Sci. Rep.* 3 (2013) 1622.
- [8] J. Chmiola, C. Largeot, P. Taberna, P. Simon, Y. Gogotsi, *Science* 328 (2010) 480.
- [9] C. Yue, Y. Yu, J. Yin, T. Wong, Y. Zang, J. Li, J. Kang, *J. Mater. Chem. A* 1 (2013) 7896.
- [10] L. Hu, H. Wu, F. Mantia, Y. Yang, Y. Cui, *ACS Nano* 4 (2010) 5843.
- [11] L. Hu, M. Pasta, F. Mantia, L. Cui, S. Jeong, H. Deshazer, J. Choi, S. Han, Y. Cui, *Nano Lett.* 10 (2010) 708.
- [12] X. Cai, M. Peng, X. Yu, Y.P. Fu, D.C. Zou, *J. Mater. Chem. C* 2 (2014) 1184.
- [13] M. Hamed, R. Forchheimer, O. Ingnas, *Nat. Mater.* 6 (2007) 357.
- [14] X. Fan, Z.Z. Chu, F.Z. Wang, C. Zhang, L. Chen, Y.W. Tang, D.C. Zou, *Adv. Mater.* 20 (2008) 592.
- [15] D.C. Zou, D. Wang, Z.Z. Chu, Z.B. Lv, X. Fan, *Coord. Chem. Rev.* 254 (2010) 1169.
- [16] B.O. Connor, K.H. An, Y. Zhao, K.P. Pipe, M. Shtein, *Adv. Mater.* 19 (2007) 3897.
- [17] Y. Qin, X.D. Wang, Z.L. Wang, *Nature* 451 (2008) 809.
- [18] J. Bae, M. Song, Y. Park, J. Kim, M.L. Liu, Z.L. Wang, *Angew. Chem. Int. Ed.* 50 (2011) 1683.
- [19] J. Ren, L. Li, C. Chen, X. Chen, Z. Cai, L. Qiu, Y. Wang, X. Zhu, H. Peng, *Adv. Mater.* 25 (2013) 1155.
- [20] K. Wang, Q. Meng, Y. Zhang, Z. Wei, M. Miao, *Adv. Mater.* 25 (2013) 1494.
- [21] Y. Fu, X. Cai, H. Wu, Z. Lv, S. Hou, M. Peng, X. Yu, D. Zou, *Adv. Mater.* 24 (2012) 5713.
- [22] B. Liu, D. Tan, X. Wang, D. Chen, G. Shen, *Small* 9 (2013) 1998.
- [23] X.Y. Wang, L. Liu, X.Y. Wang, L.H. Yi, C.Y. Hu, X.Y. Zhang, *Mater. Sci. Eng. B* 176 (2011) 1232.
- [24] K.W. Park, *J. Mater. Chem. A* 2 (2014) 4292.
- [25] S.L. Chen, F. Liu, Q.J. Xiang, X.H. Feng, G.H. Qiu, *Electrochim. Acta* 106 (2013) 360.
- [26] J. Wang, G. Zhu, L. Deng, L. Kang, Z. Hao, Z. Liu, *CrystEngComm* 14 (2012) 8253.
- [27] X.Y. Lang, A. Hirata, T. Fujita, M. Chen, *Nat. Nanotechnol.* 6 (2011) 232.
- [28] Y. He, W. Chen, X. Li, Z. Zhang, J. Fu, C. Zhao, E. Xie, *ACS Nano* 7 (2013) 174.
- [29] L. Yang, S. Cheng, Y. Ding, X. Zhu, Z.L. Wang, M.L. Liu, *Nano Lett.* 12 (2011) 321.
- [30] Q. Wang, X. Wang, B. Liu, G. Yu, X. Hou, D. Chen, G. Shen, *J. Mater. Chem. A* 1 (2013) 2468.
- [31] X. Lu, X. Huang, S. Xie, T. Zhai, C. Wang, P. Zhang, M. Yu, W. Li, C. Liang, Y. Tong, *J. Mater. Chem.* 22 (2012) 13357.
- [32] Y. Horng, Y. Lu, Y. Hsu, C. Chen, L. Chen, K. Chen, *J. Power Sources* 195 (2010) 4418.



Bin Liu is a Postdoctoral Researcher at Pacific Northwest National Laboratory (PNNL). He received his Ph.D. degree from Huazhong University of Science and Technology (HUST) in 2014. His research interest covers new-generation energy storage devices based on creative electrodes, such as flexible/wearable Li-ion batteries, fiber supercapacitors, alternative Mg-ion batteries, etc.



Boyang Liu is currently a Ph.D. candidate at University of Maryland, College Park. He received his B.E. degree from Huazhong University of Science and Technology in 2014. His research focuses on synthesis and design of flexible energy storage devices and their simulations.



Xianfu Wang received his Bachelor's degree from Jiangsu University in 2010. He is currently a Ph.D. candidate at Huazhong University of Science and Technology. His current research focuses on the design and synthesis of three dimensional nanostructures, and investigation of their fundamental properties and potential applications in flexible energy storage devices and integrated devices.



Di Chen received her B.S. degree (1999) in Chemistry from Anhui Normal University and Ph.D. degree (2005) in Chemistry from the University of Science and Technology of China. She is currently a Professor at the Huazhong University of Science and Technology. Her research interests focus on designing nanostructures for sustainable energy applications, including energy storage, solar cell, and photocatalysts.



Zhiyong Fan received his B.S. and M.S. degree in physical electronics from Fudan University, Shanghai, China, in 1998 and 2001. He received Ph.D. degree from University of California, Irvine in 2006 in Materials Science. In May 2010, he joined Hong Kong University of Science and Technology as an assistant professor. His current research includes fabrication and characterization of nanomaterials and nanostructures; applications of functional nanomaterials for electronics, energy harvesting and sensing.



Guozhen Shen received his B.S. degree (1999) in Chemistry from Anhui Normal University and Ph.D. degree (2003) in Chemistry from University of Science and Technology of China. He joined the Institute of Semiconductors, Chinese Academy of Sciences as a Professor in 2013. His current research focused on flexible electronics and printable electronics, including transistors, photodetectors, sensors and flexible energy storage and conversion devices.